Journal of Catalysis 286 (2012) 214–223

Contents lists available at SciVerse ScienceDirect

Journal of Catalysis

journal homepage: www.elsevier.com/locate/jcat

Solvation and acid strength effects on catalysis by faujasite zeolites

Rajamani Gounder [a], Andrew J. Jones [a], Robert T. Carr [a], Enrique Iglesia [a,b,*]

[a] Department of Chemical Engineering, University of California at Berkeley, Berkeley, CA 94720, United States
[b] Division of Chemical Sciences, E.O. Lawrence Berkeley National Laboratory, Berkeley, CA 94720, United States

ARTICLE INFO

Article history:
Received 1 July 2011
Revised 28 October 2011
Accepted 6 November 2011
Available online 14 December 2011

Keywords:
Acid strength
Faujasite
Isobutane
Sodium
Solvation

ABSTRACT

Kinetic, spectroscopic, and chemical titration data indicate that differences in monomolecular isobutane cracking and dehydrogenation and methanol dehydration turnover rates (per H^+) among FAU zeolites treated thermally with steam (H-USY) and then chemically with ammonium hexafluorosilicate (CD-HUSY) predominantly reflect differences in the size and solvating properties of their supercage voids rather than differences in acid strength. The number of protons on a given sample was measured consistently by titrations with Na^+, with CH_3 groups via reactions of dimethyl ether, and with 2,6-di-*tert*-butylpyridine *during* methanol dehydration catalysis; these titration values were also supported by commensurate changes in acidic OH infrared band areas upon exposure to titrant molecules. The number of protons, taken as the average of the three titration methods, was significantly smaller than the number of framework Al atoms (Al_f) obtained from X-ray diffraction and ^{27}Al magic angle spinning nuclear magnetic resonance spectroscopy on H-USY (0.35 H^+/Al_f) and CD-HUSY (0.69 H^+/Al_f). These data demonstrate that the ubiquitous use of Al_f sites as structural proxies for active H^+ sites in zeolites can be imprecise, apparently because distorted Al structures that are not associated with acidic protons are sometimes detected as Al_f sites. Monomolecular isobutane cracking and dehydrogenation rate constants, normalized non-rigorously by the number of Al_f species, decreased with increasing Na^+ content on both H-USY and CD-HUSY samples and became undetectable at sub-stoichiometric exchange levels (0.32 and 0.72 Na^+/Al_f ratios, respectively), an unexpected finding attributed incorrectly in previous studies to the presence of minority "super-acidic" sites. These rate constants, when normalized rigorously by the number of residual H^+ sites were independent of Na^+ content on both H-USY and CD-HUSY samples, reflecting the stoichiometric replacement of protons that are uniform in reactivity by Na^+ cations. Monomolecular isobutane cracking and dehydrogenation rate constants (per H^+; 763 K), however, were higher on H-USY than CD-HUSY (by a factor of 1.4). Equilibrium constants for the formation of protonated methanol dimers via adsorption of gaseous methanol onto adsorbed methanol monomers, determined from kinetic studies of methanol dehydration to dimethyl ether (433 K), were also higher on H-USY than CD-HUSY (by a factor of 2.1). These larger constants predominantly reflect stronger dispersive interactions in H-USY, consistent with its smaller supercage voids that result from the occlusion of void space by extraframework Al (Al_{ex}) residues. These findings appear to clarify enduring controversies about the mechanistic interpretation of the effects of Na^+ and Al_{ex} species on the catalytic reactivity of FAU zeolites. They also illustrate the need to normalize rates by the number of active sites instead of more convenient but less accurate structural proxies for such sites.

1. Introduction

Faujasite (FAU, Y-zeolite) is used as a solid acid catalyst, often after thermal or chemical treatments render it more stable during catalysis [1–4]. Although FAU zeolites contain only one framework Al (Al_f) T-site, isolated Al_f atoms give rise to OH groups with significantly smaller deprotonation energies (DPE; 1161–1166 kJ mol^{-1}) than OH groups on Al_f atoms with next-nearest Al neighbors (1177–1247 kJ mol^{-1}) [5]. As a result, isolated *Brønsted acid sites* in FAU zeolites should behave as uniform sites, equal in acid strength as well as solvating environment. This appears to be consistent with rates of alkane cracking (per g) that are proportional to the number of isolated *Al_f atoms* on FAU zeolites treated by a given thermal or chemical protocol [6–10]. Yet, cracking rates (per Al_f) differ among FAU zeolites treated by different thermal and chemical methods [6–10], in apparent contradiction to the constant turnover rates expected from a single-site catalyst.

Thermal treatments that convert Y-zeolite to its ultrastable form (USY) [1,4,11,12] create extraframework Al (Al_{ex}) moieties by the extraction of Al from framework sites and also increase

* Corresponding author at: Department of Chemical Engineering, University of California at Berkeley, Berkeley, CA 94720, United States. Fax: +1 510 642 4778.
E-mail address: iglesia@berkeley.edu (E. Iglesia).

0021-9517/$ - see front matter © 2011 Elsevier Inc. All rights reserved.
doi:10.1016/j.jcat.2011.11.002

cracking rates (per g) of *i*-C_4H_{10} [7], *n*-C_5H_{12} [9], and *n*-C_6H_{14} [6,13,14]. Alkane cracking reactions are fully suppressed upon addition of only small amounts of Na^+ to H-USY (0.2–0.3 per Al_f) [9,15–17]. These effects have been previously interpreted as the result of a small number of highly reactive and "super-acidic" Brønsted sites, formed via electronic interactions with Al_{ex} moieties and titrated selectively by Na^+ [9,15–17]. Some studies have alternatively suggested that higher alkane cracking rates on thermally-treated zeolites reflect the generation of mesopores and external surfaces that decrease diffusional constraints on bimolecular cracking reactions [13,18–21]. A recent study concluded that monomolecular C_3H_8 cracking turnovers occur only on H^+ sites at isolated Al_f atoms [10]; however, this interpretation appears inconsistent with turnover rates (per H^+) that vary (up to factors of 3) on FAU zeolites treated with steam, ammonia, or ethylenediaminetetraacetic acid [10] and with the elimination of detectable alkane cracking rates after substoichiometric titration of isolated Al_f with Na^+ cations [15–17].

Here, we examine the structural and catalytic properties of FAU zeolites containing different Al_f and Al_{ex} contents, resulting from thermal treatment in water vapor that forms Al_{ex} moieties and from chemical treatments with $(NH_4)_2SiF_6$ that remove these species. The number of H^+ was determined directly by their chemical titration with Na^+, with dimethyl ether (DME) to form CH_3 groups, and with 2,6-di-*tert*-butylpyridine *during* methanol dehydration catalysis. On each sample, proton counts were similar among these methods but much smaller than the number of Al_f atoms, determined by ^{27}Al magic angle spinning nuclear magnetic resonance (MAS NMR) spectroscopy and X-ray diffraction (XRD). Yet, Al_f atoms measured by these methods are ubiquitously used as structural proxies for Brønsted acid sites in the reporting of catalytic reactivity as turnover rates.

Turnover rates (per H^+) for isobutane cracking and dehydrogenation (763 K) and methanol dehydration to DME (433 K) were measured at differential conversions in the absence of mass and heat transfer artifacts. These kinetic data provide evidence that Na^+ cations stoichiometrically titrate H^+ sites that are uniform in reactivity and acid strength within a given sample. These data also indicate that thermal and chemical treatments predominantly influence the solvation properties of FAU supercage voids rather than the strength of Brønsted acid sites. These findings seem to resolve issues that have persisted for decades regarding the mechanistic origin of the effects of Na^+ and Al_{ex} species in catalysis by FAU zeolites. The distractions inherent in using imprecise structural proxies (Al_f) for active sites (H^+) to normalize reaction rates have led to incorrect interpretations of reactivity in terms of "super-acid" sites.

2. Methods

2.1. Catalyst synthesis and preparation

H-USY (Engelhard, Si/Al = 2.8), H-BEA (Zeolyst, Si/Al = 11.8), and H-MFI (Zeolyst, Si/Al = 16.5) samples were treated in flowing dry air (2.5 $cm^3\ g^{-1}\ s^{-1}$, zero grade, Praxair) by heating to 773 K (at 0.0167 K s^{-1}) and holding for 4 h. A chemically-dealuminated USY sample (CD-NH_4USY, Si/Al_{tot} = 7.5) was prepared by protocols reported in the LZ-210 patent [22]; this procedure has been shown to remove Al_{ex} moieties selectively without significant removal of Al_f atoms [23]. H-USY (Union Carbide, Si/Al = 2.9, 12 kg) was stirred in H_2O (36 L) at 348 K while adding an aqueous 1.5 M $(NH_4)_2SiF_6$ solution (99%, 15 L, 323 K) continuously (at 1.67 g s^{-1}). Small batches (1.8 kg) of this treated zeolite slurry were then added to aqueous $Al_2(SO_4)_3$ solutions (0.6 M, 0.8 L) and stirred at 368 K for 24 h to decrease the fluoride content in the samples. The resulting solids were filtered and rinsed with 1 L H_2O (per kg solid) to yield CD-NH_4USY. CD-HUSY was obtained by treating CD-NH_4USY in flowing dry air (2.5 $cm^3\ g^{-1}\ s^{-1}$, zero grade, Praxair) by heating to 773 K (at 0.0167 K s^{-1}) and holding for 4 h to convert NH_4^+ to H^+. H-USY and CD-HUSY samples were exposed to ambient air before structural and functional characterization.

H-USY, NH_4-CD-USY, and CD-HUSY samples (0.5–2.0 g) were partially-exchanged with Na^+ cations by stirring in aqueous $NaNO_3$ (99%, EMD Chemicals) solutions (0.25 or 0.50 L) at 353 K for 12 h. The extent of Na^+ exchange was varied by changing the concentration of $NaNO_3$ in the exchange solution (0.001–0.150 M). These Na^+-exchanged zeolites were filtered and rinsed with 1 L of deionized H_2O. Na^+-zeolites were treated in flowing dry air (2.5 $cm^3\ g^{-1}\ s^{-1}$, zero grade, Praxair) by heating to 773 K (at 0.0167 K s^{-1}) and holding for 4 h to convert residual NH_4^+ cations to H^+. Samples were exposed to ambient air before structural and functional characterization studies.

2.2. Catalyst characterization

Al_f and Al_{ex} contents were estimated from XRD and ^{27}Al MAS NMR spectroscopy. X-ray diffractograms of zeolite samples, after exposure to ambient air, were obtained using a Siemens D-5000 diffractometer and Cu Kα radiation. Lattice parameters were calculated from (5 3 3) reflections and were used to estimate Al_f content based on methods reported in the literature [24,25] (diffractograms and additional details in Section S.1, Supporting information). ^{27}Al MAS NMR spectra of zeolites were collected using a Bruker Avance 500 MHz spectrometer in a wide-bore 11.7 Tesla magnet (Caltech Solid State NMR Facility). Samples were held within a 4 mm ZrO_2 rotor and hydrated in a desiccator containing 1.0 M KCl for >48 h before sealing the rotor. NMR spectra were measured at 130.35 MHz using a 4 mm cross-polarization (CP) MAS probe with the application of strong proton decoupling and with a magic angle spinning rate of 13 kHz. NMR spectra were acquired at ambient temperature from 512 scans with 0.5 μs pulses and a 6 s delay. All NMR spectra were referenced to aqueous 1.0 M $Al(NO_3)_3$ solutions.

The number and types of OH groups remaining after titration with different amounts of Na^+ or pyridine were determined from the intensity of OH vibrational bands (3400–3800 cm^{-1}) before and after titrant introduction. Infrared (IR) spectra were collected with a Nicolet NEXUS 670 Fourier-transform spectrometer equipped with a Hg–Cd–Te (MCT) detector by averaging 64 scans at 2 cm^{-1} resolution in the 4000–400 cm^{-1} range. Self-supporting wafers (5–15 mg cm^{-2}) were sealed within a quartz vacuum cell equipped with NaCl windows, treated in flowing dry air (1.67 $cm^3\ s^{-1}$, zero grade, Praxair) at 773 K (at 0.033 K s^{-1}) and holding for 2 h, evacuated at 773 K for >2 h (<0.01 Pa dynamic vacuum; Edwards E02 diffusion pump) and cooled to 303 K in vacuum before collecting spectra. Acid sites were titrated with pyridine (99.8%, Aldrich) at 298 K and 450 K by incremental dosing without intervening evacuation; infrared spectra were collected after each dose. All infrared spectra were normalized by overtone and combination bands for zeolite framework vibrations (1750–2100 cm^{-1}).

Total Si, Al and Na contents were determined by inductively-coupled plasma optical emission spectroscopy (Galbraith Laboratories).

2.3. Methylation of OH groups by dimethyl ether

The number of protons on each zeolite sample was measured by titration with dimethyl ether. Samples were placed in a quartz tube (7.0 mm i.d.) held at 438 K using a resistively heated three-zone furnace (Applied Test Systems Series 3210) and Watlow controllers (EZ-ZONE PM Series). Samples (0.10–0.12 g, 180–250 μm) were

held on a coarse quartz frit; temperatures were measured with a K-type thermocouple contained within a thermowell at the external tube surface.

Samples were treated in a flowing 5% O_2/He mixture (8.3 $cm^3\ g^{-1}\ s^{-1}$, 99.999%, Praxair) by heating to 773 K (at 0.025 K s^{-1}) and holding for 2 h, followed by cooling to 438 K (at 0.083 K s^{-1}) in flowing He (16.7 $cm^3\ g^{-1}\ s^{-1}$, 99.999%, Praxair). DME reactants (0.30 $cm^3\ s^{-1}$, 99.8%, Praxair) were treated by passing over CaH_2 (99%, Aldrich) at ambient temperature to remove trace amounts of water and mixed with Ar (0.15 $cm^3\ s^{-1}$, 99.999%, Praxair), used as an inert tracer, before flowing through a sample loop (420 K, 0.250 cm^3). This DME/Ar mixture was introduced onto samples as pulses through heated transfer lines (420 K), via injection into flowing He (14.2 $cm^3\ s^{-1}\ g^{-1}$, 99.999%, Praxair) at 10 s intervals. A heated Si-coated stainless steel capillary (420 K, 0.254 mm i.d., 183 cm length) placed at the end of the quartz frit holding the samples brought the effluent into a mass spectrometer (MKS Spectra Minilab) to measure the concentrations of DME (m/z = 45, 46), CH_3OH (m/z = 32), H_2O (m/z = 18) and Ar (m/z = 40) every 0.7 s.

2.4. Isobutane reaction rates and selectivities

Isobutane cracking and dehydrogenation rates were measured at differential conversions (<2%) in a tubular packed-bed quartz reactor (7.0 mm i.d.) with plug-flow hydrodynamics at 763 K. Samples (0.01–0.05 g, 180–250 μm) were held on a coarse quartz frit. Temperatures were set by a resistively-heated three-zone furnace (Applied Test Systems Series 3210) and Watlow controllers (96 Series) and measured with a K-type thermocouple held within a thermowell at the external surface of the quartz tube.

Catalysts were treated in 5% O_2/He flow (16.7 $cm^3\ g^{-1}\ s^{-1}$, 99.999%, Praxair) by heating to 803 K (at 0.0167 K s^{-1}) and holding for 2 h. This stream was replaced with He (16.7 $cm^3\ g^{-1}\ s^{-1}$, 99.999%, Praxair) for 0.5 h, while isobutane (10% i-C_4H_{10}, 5% Ar, 85% He, Praxair, 99.5% purity) was sent to a gas chromatograph (Agilent HP-6890GC) via heated lines (423 K) for calibration purposes. Reactant pressures (0.1–1.0 kPa i-C_4H_{10}) and inlet molar rates (10^{-6}–10^{-4} (mol i-C_4H_{10}) $g^{-1}\ s^{-1}$) were varied by diluting with inert He (99.999%, Praxair). Reactant and product concentrations were measured by flame ionization and thermal conductivity detectors after chromatographic separation (GS-AL/KCl Agilent capillary column, 0.530 mm ID × 50 m; HayeSep DB Sigma–Aldrich packed column, 100–120 mesh, 10 ft.). Rates and selectivities measured after ~12 h on stream were similar (within 5%) to initial steady-state values on all samples, indicating that rate and selectivity data were not affected by changes in the number, reactivity, or accessibility of active sites.

2.5. Methanol dehydration rates and titration of H^+ with 2,6-di-tert-butyl pyridine during catalysis

CH_3OH dehydration rates to dimethyl ether were measured at differential conversions (<2%) at 433 K in the reactor setup described in Section 2.3. Catalyst samples (0.01–0.05 g, 125–180 μm) were diluted with SiO_2 (Cab-o-sil, washed with 1.0 M HNO_3, 125–180 μm, >0.1 g total bed weight) and treated in dry air (99.999%, Praxair) by heating to 773 K (at 0.083 K s^{-1}) and holding for 2 h. Liquid CH_3OH (99.8%, Sigma–Aldrich; no additional purification) was evaporated into a stream of He (99.999%, Praxair) using a liquid syringe pump (Cole-Palmer 780200C series) and transferred via heated lines (>393 K) to prevent the condensation of liquids. Reactant pressures (0.02–22 kPa CH_3OH) and inlet molar rates were changed by varying liquid flow rates. Concentrations of reactants, products, and titrants were determined by gas chromatography (Agilent 6890 N GC) using flame ionization detection (DB-Wax capillary column; 0.320 mm ID × 30 m × 0.25 μm film; J&W Scientific) and mass spectrometry (MKS Spectra Minilab). Dimethyl ether and water were the only products observed under all reaction conditions examined. SiO_2 (0.1 g) did not lead to detectable product formation at the conditions used in this study. Conditions were periodically returned to a reference condition (0.6 kPa CH_3OH, 433 K) to check for catalyst deactivation during kinetic experiments. Rates were similar to initial values at the reference condition for H-BEA and H-MFI (within 5% after 6 h time-on-stream) indicating that deactivation was negligible on these samples. Rates at the reference condition decreased systematically by ~40% and ~15% on H-USY and CD-HUSY, respectively, over 6 h time-on-stream and were corrected using periodic rate measurements at the reference condition (details in Section S.2, Supporting information).

The number of Brønsted acid sites on H-USY, CD-HUSY and H-BEA was measured by titration with 2,6-di-*tert*-butyl pyridine during dehydration catalysis in the same reactor setup. Steady-state dehydration rates at 433 K were maintained before the introduction of titrant molecules. 2,6-di-*tert*-Butylpyridine (>97%, Aldrich; no additional purification) was dissolved in CH_3OH (99.8%, Sigma–Aldrich) reactants and evaporated into a He stream (99.999%, Praxair) using a syringe pump to give their desired concentrations (0.40–0.55 Pa titrant). Titrant adsorption uptakes and dehydration rates were calculated during titrant injection from the concentrations of reactants, products, and titrants in the reactor effluent using the chromatographic protocols described above. The total number of protons on each sample was calculated by extrapolating cumulative titrant uptake to zero dehydration rates and assuming 1:1 titrant:H^+ adsorption stoichiometries [26]. Titrations using pyridine (99.8%, anhydrous, Aldrich) were conducted using the same protocols over a range of 0.30–3.0 Pa of pyridine.

3. Results and discussion

3.1. Characterization of aluminum structure and coordination in zeolites

Catalytic rates on acidic zeolites are often normalized by the number of framework Al atoms, which act as structural surrogates for protons that are assumed to exist in equimolar amounts to balance the framework negative charge. The different ^{27}Al MAS NMR lines for tetrahedral Al_f and octahedral Al_{ex} atoms (60 and 0 ppm chemical shifts) can be used to distinguish these species, but Al centers in distorted environments give broad lines that often become undetectable [27,28]. ^{27}Al MAS NMR spectra for H-USY, CD-HUSY, and CD-NH_4USY, acquired after hydrating samples (Section 2.2), are shown in Fig. 1. CD-NH_4USY gave much sharper tetrahedral Al lines than H-USY (Fig. 1) and the latter, but not the former, showed a line at 0 ppm corresponding to octahedral Al centers. These spectra indicate that treatment of H-USY with $(NH_4)_2SiF_6$ either removed Al centers in octahedral and distorted tetrahedral sites or converted them to tetrahedral Al centers through healing of structural defects. An octahedral Al NMR line appears in the spectrum of CD-HUSY (Fig. 1) upon removal of NH_4 by treatment in dry air at 773 K and subsequent exposure to ambient conditions. This reflects either the complete extraction of some Al_f atoms into Al_{ex} moieties or the presence of coordinatively-unsaturated Al species that can reversibly change between tetrahedral and octahedral coordination depending on the temperature and the identity of the coordinating species (e.g., H_2O, NH_3) [29,30].

The fraction of the total Al atoms present as Al_f species was estimated from the integrated intensities of tetrahedral and octahedral Al NMR lines in the spectra shown in Fig. 1; their values are 0.71 on

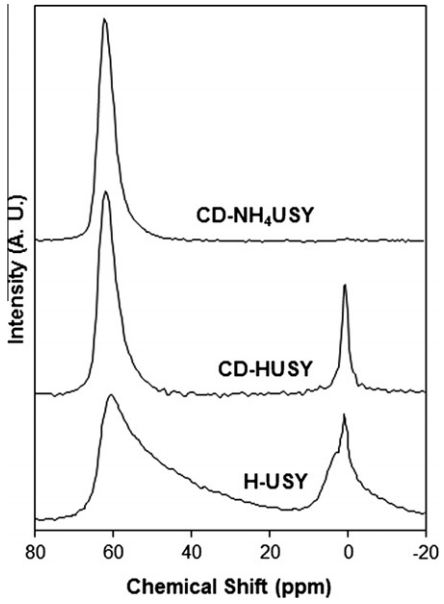

Fig. 1. ^{27}Al MAS NMR spectra of H-USY, CD-HUSY, and CD-NH_4USY; chemical shifts referenced to $Al(NO_3)_3$.

Table 1
Elemental composition and structural characterization of zeolite samples.

Zeolite	Si/Al_{tot}[a]	Al_f/Al_{tot}		Si/Al_f[b]	Al_{ex}/supercage[c]
		^{27}Al MAS NMR	XRD		
H-USY	2.8	0.71	0.46	6.1	<3.9
CD-HUSY	7.5	0.75	0.74	10.1	<0.76
CD-NH_4USY	7.5	0.99	n.m.*	7.5	<0.03

[a] Determined from elemental analysis (ICP-OES; Galbraith Laboratories).
[b] Determined from XRD for H-USY and CD-HUSY (details in Section S.1, Supporting information) and from ^{27}Al MAS NMR for CD-NH_4USY (supporting text in Section 3.1).
[c] Upper bound for Al_{ex} content (per supercage) estimated from Al_f (by XRD or NMR) and Al_{tot} (by elemental analysis) contents (details in Section S.1, Supporting information).
* n.m., not measured.

H-USY and 0.75 on CD-HUSY (Table 1). The number of Al_f atoms can also be inferred from XRD-derived FAU lattice constants because Al–O bonds are longer than Si–O bonds [24,25]; these methods (details and diffractograms in Section S.1, Supporting information) gave Al_f/Al_{tot} ratios of 0.46 on H-USY and 0.74 on CD-HUSY (Table 1). Estimates of Al_f content may be imprecise, however, because some Al atoms may not be detected in NMR spectra or may reside within distorted tetrahedral locations and in extrazeolite phases. The *ex situ* conditions of these measurements, such as the hydration treatments at ambient temperature intended to weaken Al quadrupolar interactions and sharpen NMR lines, may also cause unintended structural changes that may be reversed at the conditions used for catalysis. Ultimately, Al_f atoms are merely a structural surrogate for active sites, which are present as charge-balancing protons (H^+). As we show next, these sites can be counted directly and precisely at conditions relevant to catalysis using chemical titrants.

3.2. Titration of Brønsted acid sites in zeolites

The number of H^+ (or NH_4^+) on H-USY, CD-HUSY, and CD-NH_4USY was determined by equilibrium exchange with Na^+ [31] under aqueous conditions at 353 K (Section 2.1) according to:

$$Na^+_{aq} + [SiO^-(X^+)Al] \overset{K_X}{\longleftrightarrow} X^+_{aq} + [SiO^-(Na^+)Al], \quad (1)$$

where X^+ denotes the cation (H^+ or NH_4^+) present initially at anionic framework oxygen sites (Al_{exch}). The number of X^+ cations replaced as a function of Na^+ concentration in solution is described by the isotherm:

$$\theta_{Na^+} = \frac{Na^+}{Al_{tot}} = \left(\frac{Al_{exch}}{Al_{tot}}\right) \frac{K_X (Na^+)_{aq}/(X^+)_{aq}}{1 + K_X (Na^+)_{aq}/(X^+)_{aq}}, \quad (2)$$

in which K_X is the equilibrium constant for the replacement of X^+ by Na^+ (derivation in Section S.3, Supporting information). Here, θ_{Na^+} reflects the Na^+/Al_{tot} ratio after exchange, determined by elemental analysis; these values are plotted for H-USY, CD-HUSY, and CD-NH_4USY against aqueous-phase Na^+/X^+ ratios in Fig. 2. Saturation Na^+ exchange levels (Al_{exch}/Al_{tot}) were determined from Na^+ exchange data by regression to the form of Eq. (2). The difference between saturation Na^+ levels and Na^+ contents in partially-exchanged samples was taken as the number of residual H^+ sites after Na^+-exchange.

Saturation Na^+ exchange levels (per Al_{tot}) were 0.28 on H-USY and 0.51 on CD-HUSY (Table 2), indicating that only a fraction of all the Al atoms contain a proton that can be exchanged by Na^+. These values were larger for CD-NH_4USY (0.85 Na^+/Al_{tot}; Table 2) than for CD-HUSY, suggesting that NH_4 removal by treatment in dry air at 773 K and subsequent exposure to ambient air to form CD-HUSY led to framework dealumination [3,32], which decreased the number of available exchange sites and, in turn, the number of protons available for exchange.

Infrared spectra of CD-HUSY and two Na^+-exchanged CD-HUSY samples are shown in Fig. 3 (spectra of all CD-HUSY samples in Section S.4, Supporting information). They showed strong bands at 3630 and 3550 cm^{-1}, assigned to acidic OH groups vibrating within supercage and sodalite cages, respectively; weaker bands at 3740 cm^{-1} (silanol OH) and 3675 cm^{-1} (OH associated with Al_{ex} species) were also detected [10,33]. The intensity of the acidic OH bands decreased linearly with increasing Na^+/Al_{tot} ratio (Fig. 3 inset) and extrapolated to zero values at 0.56 Na/Al_{tot} ratios, consistent with the maximum ion-exchange capacity of CD-HUSY (0.51 Na/Al_{tot}; Table 2) and with the complete replacement of H^+ by Na^+.

The infrared spectra of H-USY and two Na^+-exchanged H-USY samples are shown in Fig. 4 (the other samples are included in

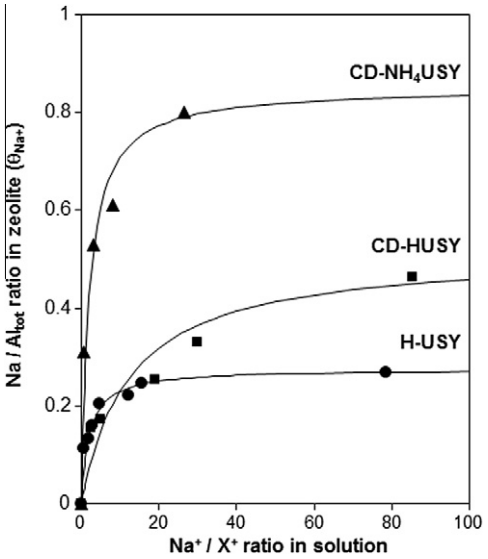

Fig. 2. Aqueous-phase Na^+-exchange isotherms (353 K) for H-USY (●), CD-HUSY (■) and CD-NH_4USY (▲), where X^+ denotes the cation initially present on zeolite samples (NH_4^+ or H^+). Solid curves represent the regressed best fits to Eq. (2). Saturation Na^+ exchange levels listed in Table 2.

Table 2
Titration of Brønsted acid sites on zeolite samples.

Zeolite	H^+/Al_{tot}			H^+/Al_f[a]	Na/Al_f at zero turnover rates[b]
	Na^+	CH_3^+	2,6 *di-tert*-butylpyridine		
H-USY	0.28	0.26	0.20	0.35	0.32 ± 0.04
CD-HUSY	0.51	0.53	0.50	0.69	0.72 ± 0.05
CD-NH_4USY	0.85	n.m.*	n.m.*	0.86	n.m.*

[a] Calculated from average H^+ count determined by the three titration methods and the Al_f count determined by ^{27}Al MAS NMR (Table 1).
[b] Extrapolated Na/Al_f ratios required for undetectable *i*-C_4H_{10} cracking and dehydrogenation rates (from Fig. 7).
* n.m., not measured.

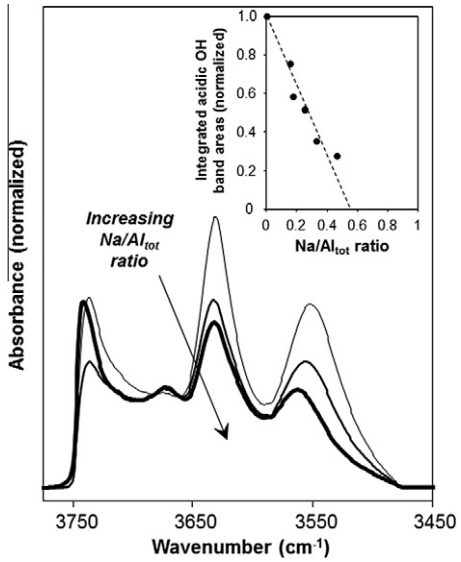

Fig. 3. IR spectra of CD-HUSY samples with increasing Na/Al_{tot} ratio (lighter to darker: 0.00, 0.25, 0.46); absorbance normalized to framework vibrations (1750–2100 cm^{-1}). Inset: Integrated acidic OH band areas (3500–3660 cm^{-1}) in difference spectra with respect to CD-HUSY (Fig. S.4) plotted as a function of Na/Al_{tot} ratio; dashed line represents line of best fit through the point at (0,1) and extrapolates to zero intensity at Na/Al_{tot} = 0.56.

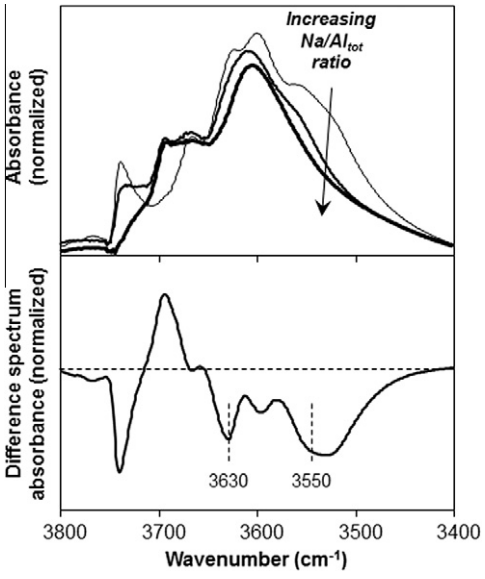

Fig. 4. Top: IR spectra of H-USY samples with increasing Na/Al_{tot} ratio (lighter to darker: 0.00, 0.16, 0.25); absorbance normalized to framework vibrations (1750–2100 cm^{-1}). Bottom: Difference spectrum of USY sample with saturation Na^+ levels (Na/Al_{tot} = 0.25) with respect to H-USY.

Section S.4, Supporting information). In contrast with CD-HUSY, saturation Na^+ levels on H-USY did not fully remove OH bands (3660–3475 cm^{-1}), which retained a strong feature at 3600 cm^{-1} (Fig. 4 top). The difference spectrum between H-USY samples before and after Na^+-exchange (Fig. 4 bottom) predominantly shows bands assigned to acidic OH groups centered at 3630 and 3550 cm^{-1} (~90% of total difference spectrum area), indicating that Na^+ preferentially titrates H^+ sites. These findings sharply contrast previous reports that Na^+ selectively replaced "super-acid" sites (but not isolated OH groups), which were assigned to a perturbed OH band at ~3600 cm^{-1} [16]. We conclude that acidic OH groups do not give rise to the band at 3600 cm^{-1}, as also proposed earlier [10], and that this band may instead reflect the presence of OH groups on amorphous extrazeolite phases [23,34] formed during thermal treatment.

The numbers of protons on H-USY and CD-HUSY were also determined by sequential pulses of DME at 438 K to replace H^+ sites with CH_3 groups [35]:

$$CH_3OCH_3 + [SiO(H)Al] \rightarrow [SiO(CH_3)Al] + CH_3OH, \quad (3)$$

$$CH_3OH + [SiO(H)Al] \rightarrow [SiO(CH_3)Al] + H_2O. \quad (4)$$

DME and CH_3OH concentrations were undetectable in the reactor effluent during the initial pulses on H-USY and CD-HUSY, consistent with the fast and irreversible nature of these methylation reactions. DME was detected in the effluent only after all protons were replaced by CH_3 groups (data in Section S.5, Supporting information), while CH_3OH was never detected in the effluent stream. DME uptakes (assuming 0.5:1 DME:H^+; Eqs. (3) and (4)) gave H^+/Al_{tot} ratios of 0.26 and 0.53 on H-USY and CD-HUSY, respectively (Table 2). These values were similar, within experimental accuracy, to the respective maximum Na^+ exchange capacities of these samples (Table 2), but much smaller than expected if each Al_f atom were associated with one proton.

Finally, the number of protons in H-USY and CD-HUSY was measured *during* CH_3OH dehydration catalysis at 433 K by their titration with 2,6-di-*tert*-butylpyridine (i.e., hindered pyridine). This base titrates only Brønsted acid sites because steric constraints around its N-atom prevent coordination to Lewis acid centers [26]. On both H-USY and CD-HUSY, CH_3OH dehydration rates remained constant with time before titrant introduction and then decreased monotonically with increasing titrant uptakes (Fig. 5). Detectable rates (~20% of initial rates) persisted on both samples even at maximum uptakes (0.17 and 0.38 titrant per Al_{tot} on H-USY and CD-HUSY, respectively). Titration of CD-HUSY with pyridine, which binds to both Brønsted and Lewis sites, gave larger maximum uptakes (0.66 pyridine per Al_{tot}) than with hindered pyridine. Residual rates at saturation uptakes were similar for both pyridine and hindered pyridine titrants (Fig. 5), however, indicating that CH_3OH dehydration occurs at nearly undetectable rates on Lewis acid centers on these samples. The infrared spectrum of CD-HUSY after adsorption of 0.71 pyridine titrants (per Al_{tot}) at 298 K, showed bands for acidic OH groups vibrating in supercages

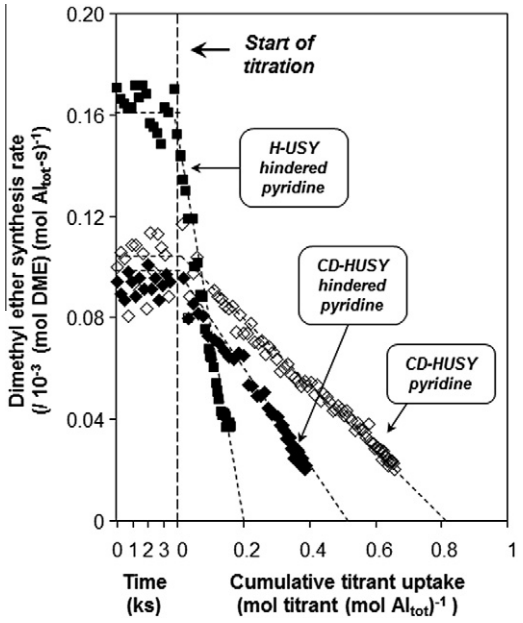

Fig. 5. Dimethyl ether synthesis rates (0.3 kPa CH_3OH, 433 K), *per total Al*, as a function time on CD-HUSY (♦) and H-USY (■) before 2,6-di-*tert*-butylpyridine introduction and on CD-HUSY before pyridine introduction (◇), and as a function of cumulative titrant uptake after titrant introduction.

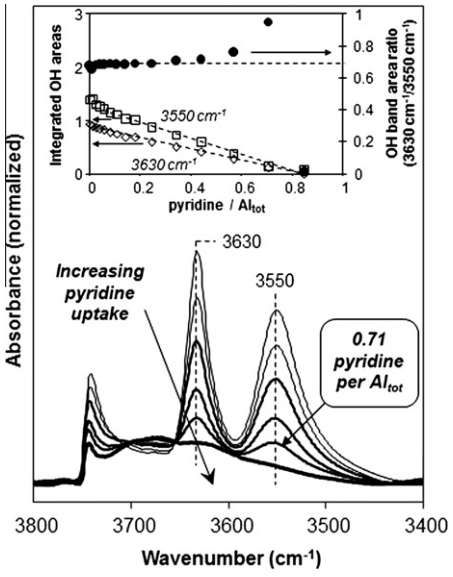

Fig. 6. IR spectra of CD-HUSY with increasing pyridine uptake (lighter to darker) at 298 K. The spectrum corresponding to a pyridine uptake (0.71 pyridine/Al_{tot}) near saturation levels during methanol dehydration catalysis (0.66 pyridine/Al_{tot}, Fig. 5) is highlighted. Inset: Integrated areas of acidic OH bands centered at 3630 cm^{-1} (◇) and 3550 cm^{-1} (□) and their ratio (●) plotted as a function of pyridine uptake.

(3630 cm^{-1}) and sodalite cages (3550 cm^{-1}) (Fig. 6). Bands for both OH groups weakened concurrently with increasing pyridine uptake (Fig. 6 inset), even though pyridine titrants cannot enter sodalite cages, because H^+ species migrate among the four O-atoms connected to each Al_f atom (further discussion in Section S.6, Supporting information).

These infrared and kinetic data indicate that residual rates of CH_3OH dehydration at saturation titrant uptakes reflect the presence of acid sites accessible to CH_3OH but not to larger titrants. Thus, the total number of acid sites that catalyze CH_3OH dehydration was determined by extrapolating hindered pyridine uptakes to zero dehydration rates, which gave values of 0.20 and 0.50 H^+ (per Al_{tot}) for H-USY and CD-HUSY, respectively (Table 2). These values are consistent with the number of H^+ measured by titration with Na^+ and DME (Table 2), but are smaller than the number of Al_f atoms determined from ^{27}Al MAS NMR spectra (Table 1). Previous studies have also reported that the number of adsorbed amine titrants on chemically-dealuminated FAU was smaller than the number of Al_f atoms determined from XRD-derived lattice constants [13].

Dehydroxylation and framework dealumination events decrease the number of protons available for titration or catalysis and form non-tetrahedral Al species that are incapable of balancing charge. H^+/Al_f ratios *decreased* monotonically (Table 2) as tetrahedral (60 ppm) lines broadened in ^{27}Al MAS NMR spectra (Fig. 1), reflecting the presence of Al centers with distorted tetrahedral or five-fold coordination [29,30,32,36] or quadrupolar broadening effects induced by Al_{ex} species proximal to Al_f sites [36,37]. These data suggest that some non-tetrahedral Al sites apparently remain detected as tetrahedral centers and, in turn, that the prevailing interpretations of ^{27}Al MAS NMR spectra can lead to imprecise estimates of the number of Al_f atoms. Yet, even precise Al_f counts would preclude rigorous determination of catalytic turnover rates because these atoms are only structural proxies for active Brønsted acid sites.

3.3. Catalytic consequences of Na^+ titration for monomolecular isobutane activation

Monomolecular reactions of isobutane over zeolitic Brønsted acid sites prevail at high temperatures and low alkene product pressures, as shown by experiment [38–40] and theory [41–43]. Catalytic sequences involve quasi-equilibrated adsorption of gaseous alkanes (A(g)) at protons (H^+Z^-) within zeolite channels (A(z)) and the subsequent protonation of C–C and C–H bonds in kinetically-relevant steps for cracking and dehydrogenation, respectively (Scheme 1) [44]. At the conditions required for monomolecular alkane activation, intrazeolite alkane concentrations are low and proportional to alkane pressures (P_A) [44] and rates are given by

$$r = K_{ads}k_{int}P_A = k_{meas}P_A, \quad (5)$$

where K_{ads} is the equilibrium constant for alkane adsorption on Brønsted acid sites, k_{int} is the intrinsic rate constant for alkane C–C or C–H bond scission, and k_{meas} is the measured first-order rate constant. Measured rate constants for isobutane cracking and dehydrogenation on H-USY and CD-HUSY did not vary with reactor residence time or with the concomitant changes in alkane conversion. Cracking led to equimolar CH_4 and C_3H_6 mixtures and dehydrogenation routes formed H_2 and isobutene; the latter isomerized to an equilibrated mixture of linear butene isomers with increasing residence time (data in Section S.7, Supporting information).

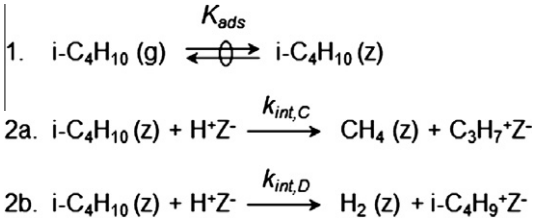

Scheme 1. Accepted pathways for monomolecular isobutane activation involve quasi-equilibrated adsorption (Step 1) from the gas phase (g) into zeolite channels (z) and subsequent reaction on Brønsted acid sites (H^+Z^-) in kinetically-relevant cracking (Step 2a) or dehydrogenation (Step 2b) steps.

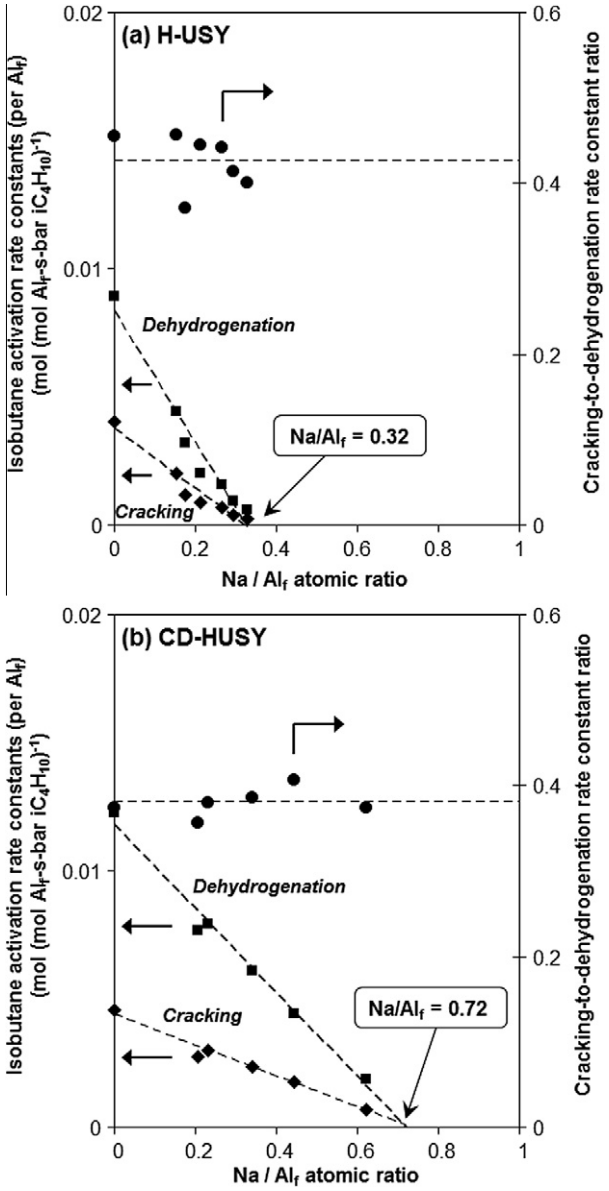

Fig. 7. Monomolecular isobutane cracking (♦) and dehydrogenation (■) rate constants (763 K), *per framework Al*, and their ratio (●) as a function of Na/Al$_f$ atomic ratio on (a) H-USY and (b) CD-HUSY.

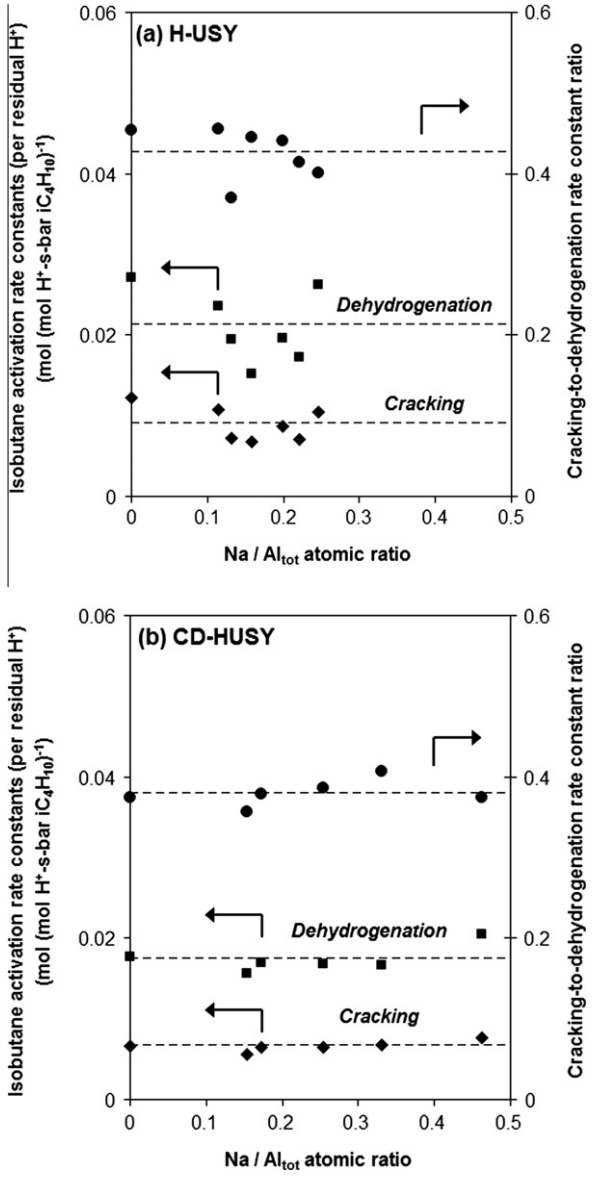

Fig. 8. First-order monomolecular isobutane cracking (♦) and dehydrogenation (■) rate constants (763 K), *per residual H$^+$*, and their ratio (●) as a function of Na/Al$_{tot}$ atomic ratio on (a) H-USY and (b) CD-HUSY.

Isobutane cracking and dehydrogenation rate constants, *normalized by the number of Al$_f$ atoms* (from ^{27}Al MAS NMR; Table 1), decreased monotonically with increasing Na$^+$ content and extrapolated to zero values at Na/Al$_f$ ratios of 0.32 on H-USY and 0.72 on CD-HUSY (Fig. 7). These strong effects of sub-stoichiometric Na$^+$ concentrations led to previous claims that Na$^+$ cations preferentially titrated uniquely active protons in H-USY, purported to become "super-acidic" as a result of stabilization of the conjugate base by Al$_{ex}$ species acting as Lewis acids [15–17] in a manner analogous to liquid superacids consisting of Brønsted–Lewis pairs. Yet, the Na/Al$_f$ ratios required to fully suppress catalytic rates on both H-USY (0.32 ± 0.04) and CD-HUSY (0.72 ± 0.05) are *identical*, within experimental accuracy, to the H$^+$/Al$_f$ ratios on these samples (0.35 and 0.69, respectively, Table 2) determined from average chemical titration values and ^{27}Al MAS NMR spectra.

Isobutane cracking and dehydrogenation rate constants, *normalized by the number of residual H$^+$*, and their ratio did not depend on Na$^+$ content on H-USY and CD-HUSY samples (Fig. 8). These data indicate that Na$^+$ cations stoichiometrically replaced all protons and that they are uniform in reactivity within each sample. Isobutane cracking and dehydrogenation rate constants (per H$^+$, 763 K), however, were larger on H-USY than on CD-HUSY (by a factor of 1.4; Table 3). These k_{meas} values measure the free energies of their respective monomolecular transition states relative to gaseous isobutane. As a result, k_{meas} values increase as acids become stronger and as zeolite voids decrease in size because transition states are stabilized more effectively by electrostatic or van der Waals forces, respectively.

Table 3
First-order rate constants ((mol (mol H$^+$-s-bar *i*-C$_4$H$_{10}$)$^{-1}$); 763 K) for monomolecular isobutane cracking ($k_{meas,C}$) and dehydrogenation ($k_{meas,D}$) and their ratio on H-USY and CD-HUSY (from Fig. 8).

Zeolite	$k_{meas,C}$	$k_{meas,D}$	$k_{meas,C}/k_{meas,D}$
H-USY	0.0090	0.021	0.43
CD-HUSY	0.0066	0.017	0.38

In the section that follows, we use methanol dehydration to dimethyl ether to assess acid strength and solvation effects on catalytic turnover rates. In contrast with monomolecular alkane activation, Brønsted acid sites need not be predominantly unoccupied for methanol dehydration routes to prevail; in turn, DME formation transition states can be measured with respect to intermediates that are similar to and different from them in charge and size, which respectively influence electrostatic and van der Waals interactions. Moreover, the comparison of methanol dehydration rates measured on zeolitic acids to those on tungsten polyoxometalate clusters, which vary widely in acid strength but for which confinement effects are absent, provide additional insight into the catalytic effects of solvation in zeolites.

3.4. Assessment of acid strength and solvation effects using methanol dehydration to dimethyl ether

Brønsted acid sites catalyze CH_3OH dehydration to DME via the quasi-equilibrated adsorption of two CH_3OH molecules to form protonated dimer intermediates; these dimers reorient to form co-adsorbed species that directly eliminate H_2O and form DME in a concerted kinetically-relevant step (Scheme 2) [45]. These elementary steps accurately describe CH_3OH dehydration on solid acid zeolites and tungsten polyoxometalate (POM) clusters with Keggin structure, with turnover rates given by (mechanistic details and derivation of rate expression in Section S.2, Supporting information) [45]:

$$\frac{r}{[H^+]} = \frac{k_{DME,d} K_C K_D P_{CH_3OH}}{1 + K_D P_{CH_3OH}}. \quad (6)$$

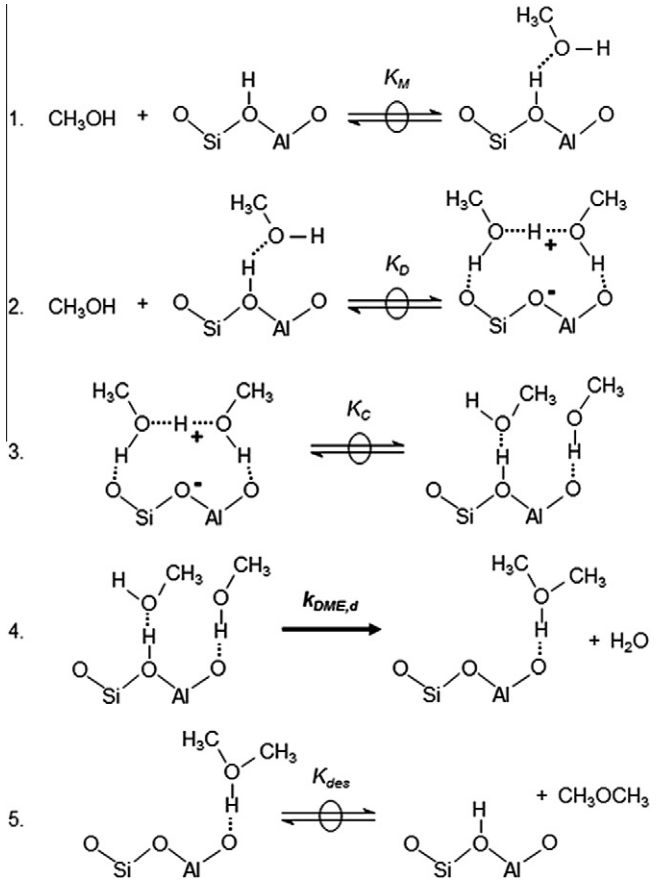

Scheme 2. Elementary steps for CH_3OH dehydration on acidic zeolites. Dashed lines represent H-bonding interactions. Adapted from Ref. [45].

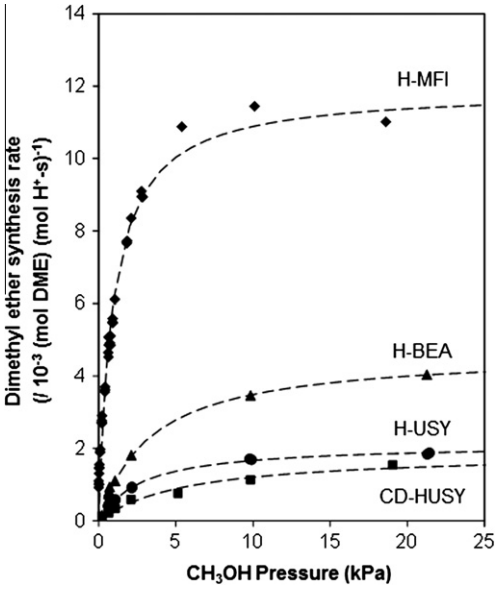

Fig. 9. Rates of dimethyl ether synthesis from CH_3OH dehydration (433 K), normalized by the number of H^+ determined from titration of H^+ by CH_3 groups, as a function of CH_3OH pressure on H-MFI (♦), H-USY (●), H-BEA (▲), and CD-HUSY (■). Dashed curves represent the regressed best fits to Eq. (6).

In this equation, $k_{DME,d}$ is the rate constant for DME formation from co-adsorbed species, and K_C and K_D are adsorption equilibrium constants for co-adsorbed methanol species and protonated methanol dimers, respectively (Scheme 2). CH_3OH dehydration rates (433 K) on H-MFI, H-BEA, H-USY, and CD-HUSY are shown as a function of CH_3OH pressure in Fig. 9, along with curves that represent the best fit of these data to the form of Eq. (6).

Values of K_D reflect the free energies of protonated CH_3OH dimers measured with respect to the combined free energies of an adsorbed CH_3OH monomer and one gaseous CH_3OH molecule [45]. Protonated CH_3OH dimers, but not uncharged CH_3OH monomers, are stabilized significantly by electrostatic interactions with the anionic conjugate base, provided here by POM clusters or aluminosilicate zeolite frameworks. As a result, differences in the stabilities of dimer and monomer intermediates, which are reflected in K_D, depend on Brønsted acid site deprotonation energy (DPE). The presence of an additional CH_3OH moiety in dimers relative to monomers also causes K_D values to depend on van der Waals interactions. These contributions become significant when active sites are confined within microporous zeolite voids but not when located on Keggin POM clusters supported on amorphous silica, for which confinement effects are small and the same for all clusters.

Values of K_D on tungsten Keggin POM clusters, whose deprotonation energies vary widely (1087–1145 kJ mol^{-1}) with differences in central atom identity (P, Si, Al, Co) [46], increased exponentially from 1.0 to 14 (kPa $CH_3OH)^{-1}$ as DPE values decreased and acid sites became stronger (Fig. 10) [45]. The value of K_D measured on H-MFI was 1.1 (kPa $CH_3OH)^{-1}$, which would require a corresponding DPE value of 1141 kJ mol^{-1} (Fig. 10) if CH_3OH dimers were *only* stabilized by electrostatic interactions. Yet, this would be an unprecedentedly low DPE value compared to those calculated (1171–1200 kJ mol^{-1}) for zeolitic acids of different framework structure (FAU, CHA, MOR, MFI) [47], indicating that electrostatic stabilization of CH_3OH dimers alone cannot account for such high K_D values on H-MFI. The K_D value for H-MFI is higher than expected (by factors of 3.5–16) for POM clusters of acid strength equivalent to those of zeolitic acids (1171–1200 kJ mol^{-1} [47]), reflecting

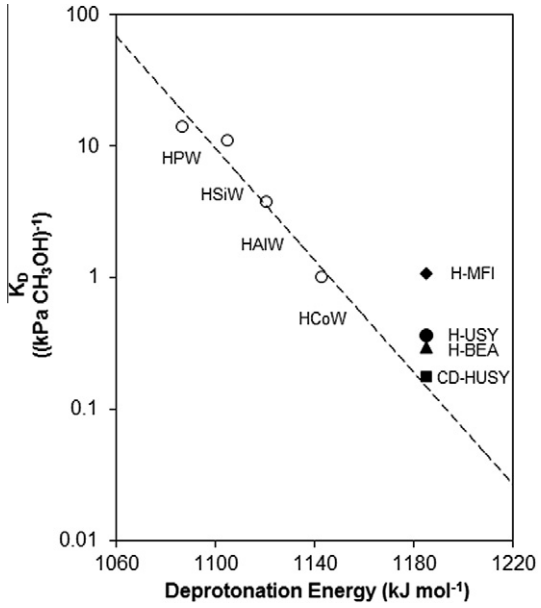

Fig. 10. Equilibrium constants for the adsorption of a CH_3OH molecule onto CH_3OH monomers to form dimers at an acid site (K_D; 433 K) as a function of deprotonation energy (DPE) for $H_{8-n}X^{n+}W_{12}O_{40}/SiO_2$ (○; central atom indicated); originally reported in [45]. Values measured for H-MFI (♦), H-USY (●), H-BEA (▲), and CD-HUSY (■) are plotted at a DPE value of 1185 kJ mol^{-1} (the center of 1170–1200 kJ mol^{-1} range reported elsewhere [47]). Dashed line represents the K_D-DPE correlation for Keggin POM clusters.

the preferential stabilization of CH_3OH dimers by van der Waals interactions in microporous H-MFI channels but not within amorphous silica supports. Indeed, theoretical studies indicate that dispersion forces stabilize CH_3OH molecules in H-MFI channels by 29 kJ mol^{-1} [48], which can account for up to ~3000-fold increases in K_D values at 433 K if concomitant losses in entropy upon confinement are neglected.

Values of K_D on all zeolitic acids (CD-HUSY, H-USY, H-BEA, H-MFI) were higher than expected (by factors of 1.2–7.6) for a POM cluster of equivalent acid strength (assuming a DPE value of 1185 kJ mol^{-1}; Fig. 10), consistent with the preferential solvation of CH_3OH dimers within microporous voids. K_D values increased systematically as void sizes decreased from CD-HUSY supercages (~1.3 nm diameter, Al_{ex}-free) to H-BEA channels (~0.7 nm diameter) to H-MFI channels (~0.5–0.6 nm diameter). These trends are consistent with dispersion interactions that also become stronger as voids become concomitantly smaller [33,49]. The value of K_D was larger on H-USY than on CD-HUSY (by a factor of 2.1, Fig. 10), suggesting that van der Waals interactions are stronger, and supercage void spaces smaller, on H-USY. At first glance, these K_D values appear to contradict the larger supercage voids expected in H-USY from its larger *unit cell size* (Table S.1, Supporting information). Direct measurements of *void size* by ^{129}Xe NMR and argon adsorption experiments, however, show that H-USY supercage voids increase in size after treatment with $(NH_4)_2SiF_6$ (to form CD-HUSY) [28,50] because these chemical treatments remove extraframework Al debris that occlude void space. The significantly higher Al_{ex} content in H-USY than in CD-HUSY (Table 1) appears to reduce effective supercage void sizes (~1.3 nm diameter, Al_{ex}-free CD-HUSY) to those similar in H-BEA channels (~0.7 nm diameter), so as to give similar K_D values on H-USY and H-BEA (Fig. 10).

These findings and their conceptual interpretations are able to resolve issues that have persisted for decades regarding the mechanistic origin of the effects of Na^+ and extraframework Al species in catalysis by FAU zeolites. They underscore the requirement that turnover rates be normalized rigorously by the number of active sites before interpreting the origins of reactivity. They also highlight the importance of measuring active sites directly and, if possible, during catalysis. In this case, the distractions of using imprecise structural surrogates (Al_f) for the active sites (H^+) to normalize rates have led to the incorrect attribution of reactivity to "super-acid" sites.

4. Conclusions

Kinetic studies of isobutane cracking and dehydrogenation (763 K) and methanol dehydration (433 K), and spectroscopic characterization of FAU zeolites treated thermally (H-USY) and then chemically with ammonium hexafluorosilicate (CD-HUSY) were used to examine the effects of extraframework aluminum (Al_{ex}) and Na^+ species on the number and strength of Brønsted acid sites. The numbers of H^+ sites on H-USY and CD-HUSY were counted directly by titration with 2,6-di-*tert*-butylpyridine *during* CH_3OH dehydration catalysis (433 K), with dimethyl ether to form CH_3 groups (438 K) and with Na^+ (353 K). These methods gave similar values for the number of protons on a given sample, which were less than the number of framework aluminum (Al_f) atoms (0.35 and 0.69 H^+/Al_f on H-USY and CD-HUSY, respectively) estimated by ^{27}Al MAS NMR. Al_f atoms are inaccurate structural proxies for Brønsted acid sites on FAU zeolites, illustrating the requirement that the number of active sites be measured directly and during catalysis.

Rate constants for monomolecular isobutane cracking and dehydrogenation, normalized rigorously by the number of residual protons on Na^+-exchanged H-USY and CD-HUSY samples, were independent of Na^+ content. These data reflect the stoichiometric replacement of catalytically-equivalent protons by Na^+ cations, in sharp contrast to previous reports [15–17] that claimed Na^+ selectively titrated "super-acidic" H^+ sites generated via electronic interactions with Al_{ex} species. These uniquely active sites were purported to comprise a small fraction of all protons on each sample, but need not be invoked to account for turnover rates normalized by the correct number of protons.

First-order rate constants for monomolecular isobutane activation (763 K), which reflect the combined effects of acid strength and solvation, were higher by a factor of 1.4 on H-USY than on CD-HUSY. Equilibrium constants for the adsorption of methanol to form protonated dimers from uncharged monomers (433 K), which increase systematically as solvation effects become stronger in zeolite voids, were higher by a factor of 2.1 on H-USY and CD-HUSY. These data indicate that van der Waals interactions are stronger within H-USY than CD-HUSY supercages, consistent with the smaller effective void sizes on the former sample, which contains larger amounts of space-occluding Al_{ex} species. Thermal and chemical treatments of FAU zeolites, which manipulate the distribution of aluminum atoms between framework and extraframework phases, change the effective sizes of supercage voids and, in turn, their solvation properties but not Brønsted acid strength.

Acknowledgments

We thank Dr. Stacey I. Zones (Chevron) and Prof. Raul F. Lobo (Univ. of Delaware) for helpful technical discussions. We also thank Roger F. Vogel (Chevron) for preparing the CD-USY sample, Dr. Sonjong Hwang (Caltech) for the ^{27}Al MAS NMR data and Dr. Jinyi Han (Chevron) for the X-ray diffractograms. We also acknowledge with thanks financial support from the Chevron Energy Technology Company for these studies. The financial support from the Chemical Sciences Division, Office of Basic Energy Sciences, Office of Sci-

ence, U.S. Department of Energy under grant number DE-FG02-03ER15479 and the supercomputing time from the Environmental Molecular Science Laboratory, a national scientific user facility sponsored by the Department of Energy's Office of Biological and Environmental Research and located at Pacific Northwest National Laboratory, is also gratefully acknowledged.

Appendix A. Supplementary material

Supplementary data associated with this article can be found, in the online version, at doi:10.1016/j.jcat.2011.11.002.

References

[1] G.T. Kerr, J. Phys. Chem. 71 (1967) 4155.
[2] G.T. Kerr, J. Phys. Chem. 72 (1968) 2594.
[3] G.T. Kerr, J. Catal. 15 (1969) 200.
[4] G.T. Kerr, J. Phys. Chem. 73 (1969) 2780.
[5] M. Sierka, U. Eichler, J. Datka, J. Sauer, J. Phys. Chem. B 102 (1998) 6397.
[6] J.R. Sohn, S.J. Decanio, P.O. Fritz, J.H. Lunsford, J. Phys. Chem. 90 (1986) 4847.
[7] R.A. Beyerlein, G.B. McVicker, L.N. Yacullo, J.J. Ziemiak, J. Phys. Chem. 92 (1988) 1967.
[8] D. Barthomeuf, Mater. Chem. Phys. 17 (1987) 49.
[9] P.V. Shertukde, W.K. Hall, J.M. Dereppe, G. Marcelin, J. Catal. 139 (1993) 468.
[10] B. Xu, S. Bordiga, R. Prins, J.A. van Bokhoven, Appl. Catal. A 333 (2007) 245.
[11] C.V. McDaniel, P.K. Maher, U.S. Pat. No. 3293,192, 1966.
[12] C.V. McDaniel, P.K. Maher, U.S. Pat. No. 3449,070, 1969.
[13] A.I. Biaglow, D.J. Parrillo, G.T. Kokotailo, R.J. Gorte, J. Catal. 148 (1994) 213.
[14] F. Lonyi, J.H. Lunsford, J. Catal. 136 (1992) 566.
[15] R.A. Beyerlein, G.B. McVicker, L.N. Yacullo, J.J. Ziemiak, Abstr. Pap.-Am. Chem. Soc. (1986) 190.
[16] P.O. Fritz, J.H. Lunsford, J. Catal. 118 (1989) 85.
[17] D. Barthomeuf, R. Beaumont, J. Catal. 30 (1973) 288.
[18] H.H. Kung, B.A. Williams, S.M. Babitz, J.T. Miller, R.Q. Snurr, Catal. Today 52 (1999) 91.
[19] B.A. Williams, J.T. Miller, R.Q. Snurr, H.H. Kung, Micropor. Mesopor. Mat. 35-6 (2000) 61.
[20] B.A. Williams, W. Ji, J.T. Miller, R.Q. Snurr, H.H. Kung, Appl. Catal. A 203 (2000) 179.
[21] B.A. Williams, S.M. Babitz, J.T. Miller, R.Q. Snurr, H.H. Kung, Appl. Catal. A 177 (1999) 161.
[22] G.W. Skeels, D.W. Breck, U.S. Pat. No. 4711,770, 1987.
[23] A. Corma, V. Fornes, F. Rey, Appl. Catal. 59 (1990) 267.
[24] J.R. Sohn, S.J. Decanio, J.H. Lunsford, D.J. O'Donnell, Zeolites 6 (1986) 225.
[25] V. Jorik, Zeolites 13 (1993) 187.
[26] C.D. Baertsch, K.T. Komala, Y.H. Chua, E. Iglesia, J. Catal. 205 (2002) 44.
[27] H. Kraus, M. Muller, R. Prins, A.P.M. Kentgens, J. Phys. Chem. B 102 (1998) 3862.
[28] R.J. Pellet, C.S. Blackwell, J.A. Rabo, J. Catal. 114 (1988) 71.
[29] A. Omegna, J.A. van Bokhoven, R. Prins, J. Phys. Chem. B 107 (2003) 8854.
[30] A. Omegna, R. Prins, J.A. van Bokhoven, J. Phys. Chem. B 109 (2005) 9280.
[31] D.W. Breck, Zeolite Molecular Sieves, John Wiley & Sons, New York, 1974.
[32] B. Xu, F. Rotunno, S. Bordiga, R. Prins, J.A. van Bokhoven, J. Catal. 241 (2006) 66.
[33] F. Eder, M. Stockenhuber, J.A. Lercher, J. Phys. Chem. B 101 (1997) 5414.
[34] V.Y. Borovkov, A.A. Alexeev, V.B. Kazansky, J. Catal. 80 (1983) 462.
[35] P. Cheung, A. Bhan, G.J. Sunley, E. Iglesia, Angew. Chem. Int. Ed. 45 (2006) 1617.
[36] J.A. van Bokhoven, A.L. Roest, D.C. Koningsberger, J.T. Miller, G.H. Nachtegaal, A.P.M. Kentgens, J. Phys. Chem. B 104 (2000) 6743.
[37] M. Hunger, G. Engelhardt, J. Weitkamp, Microporous Mater. 3 (1995) 497.
[38] R. Gounder, E. Iglesia, Angew. Chem. Int. Ed. 49 (2010) 808.
[39] E.A. Lombardo, W.K. Hall, J. Catal. 112 (1988) 565.
[40] C. Stefanadis, B.C. Gates, W.O. Haag, J. Mol. Catal. 67 (1991) 363.
[41] I. Milas, M.A.C. Nascimento, Chem. Phys. Lett. 373 (2003) 379.
[42] V.B. Kazansky, M.V. Frash, R.A. van Santen, Appl. Catal. A 146 (1996) 225.
[43] X.B. Zheng, P. Blowers, J. Phys. Chem. A 110 (2006) 2455.
[44] R. Gounder, E. Iglesia, J. Am. Chem. Soc. 131 (2009) 1958.
[45] R.T. Carr, M. Neurock, E. Iglesia, J. Catal. 278 (2011) 78.
[46] J. Macht, M.J. Janik, M. Neurock, E. Iglesia, Angew. Chem. Int. Ed. 46 (2007).
[47] M. Brändle, J. Sauer, J. Am. Chem. Soc. 120 (1998) 1556.
[48] S. Svelle, C. Tuma, X. Rozanska, T. Kerber, J. Sauer, J. Am. Chem. Soc. 131 (2009).
[49] F. Eder, J.A. Lercher, J. Phys. Chem. 100 (1996) 16460.
[50] R.L. Cotterman, D.A. Hickson, S. Cartlidge, C. Dybowski, C. Tsiao, A.F. Venero, Zeolites 11 (1991) 27.